International Journal of Heat and Mass Transfer 51 (2008) 5344–5358

Contents lists available at ScienceDirect

International Journal of Heat and Mass Transfer

journal homepage: www.elsevier.com/locate/ijhmt

The application of plastic microcapillary films for fast transient micro-heat exchange

Bart Hallmark, Christian H. Hornung, David Broady, Christopher Price-Kuehne, Malcolm R. Mackley *

Department of Chemical Engineering, New Museums Site, Pembroke Street, Cambridge CB2 3RA, UK

ARTICLE INFO

Article history:
Received 20 June 2007
Available online 29 May 2008

Keywords:
Plastic heat exchangers
Heat exchanger innovation
Micro-heat exchange
Microcapillary films
Thermal imaging

ABSTRACT

This paper reports an experimental investigation into the heat transfer response of plastic microcapillary films (MCFs). The first section presents experimental determination of temperature profiles and heat transfer coefficients for an MCF-based micro-heat exchanger. The next section presents two case studies: the first concerns cooling an electrical load, whereas the second examines heat transfer from an exothermic chemical reaction occurring within the MCF. The results demonstrate that heat transfer transients within MCF heat exchange devices are rapid. These systems provide an effective means of either heating or cooling fluids flowing within an MCF, or for removing heat from a hot surface.

1. Introduction and background

There is currently interest in the field of micro-heat exchange and its application to a variety of heat transfer problems. One area that has received attention is the cooling of computer processors; as the transistor density on these devices increases, and as their operating speeds accelerate, the thermal power dissipation rises. The need to effectively and efficiently remove this waste heat is of great importance to the stability and long-term reliability of these devices. An early investigation into on-chip liquid cooling of integrated circuits recognised that a key heat transfer constraint was the heat transfer coefficient between the heated surface and the coolant flow [1]. Further research into on-chip heat exchange includes the modelling and the creation of a design formulation for on-chip liquid heat exchanger design [2] and various designs of etched on-chip exchanger used with forced air cooling [3]. The creation of on-chip liquid cooling systems using flow impingement from micro-jets has also been studied [4] highlighting differences in the heat transfer process at the micro-scale when compared to macro-scale jet impingement. Numerical and experimental study of the use of micro-channel arrays as heat spreaders to alleviate on-chip hot spots has also been reported [5].

In these studies, the heat exchangers have been fabricated on the integrated circuit itself, using silicon as the substrate. Other studies have looked at alternative methods of cooling chips, using non-silicon based materials. One study [6] concerned the characterisation of a polymeric heat exchanger, fabricated from poly-(dimethyl siloxane) (PDMS), as an inter-chip heat exchange device for use in multiple chip packages, termed multi-chip modules.

More generally, micro-scale heat exchangers have been the focus of intense study with the advent of manufacturing techniques such as photolithography, diamond machining and other micro-machining processes. Micro-heat exchange devices tend to be characterised by high volumetric heat transfer coefficients. A laminated, cross-flow, device fabricated from diamond-machined sheets of copper foil [7] attained volumetric heat transfer coefficients of up to 44 $MW/m^3 K$. Investigation was carried out on two different designs of wire-cut micro-heat exchangers, also fabricated from copper [8]. These devices consisted of either empty deep channels or porous media filled channels and were able to achieve heat transfer coefficients of 38.4 and 86.3 $MW/m^3 K$, respectively. Theoretical studies have also been undertaken to explore the most effective micro-channel shape when faced with problem of minimising the temperature of the hot surface [9], or when optimising the micro-channel geometry with the constraints of high heat transfer and low pressure drop [10].

Micro-heat exchange devices that take advantage of phase change on the cool side have also been investigated for cooling devices that exhibit very high heat fluxes. Water has been used in micro- and mini-channels to cool electron gun accelerator targets, where heat fluxes in excess of 1 kW/cm^2 can be found [11], whereas advantage has been taken of refrigerants to achieve phase change in the coolant at lower temperatures [12].

Small liquid hold ups, and large volumetric heat transfer coefficients, can lead to fast transient responses within micro-heat exchangers [13]. Fast transient heat transfer response makes these devices attractive for use in areas of science and engineering that fall outside of microelectronics cooling. One such application, DNA amplification, is carried out by a process termed the polymerase chain reaction, or PCR [14], which involves the rapid thermal

* Corresponding author.
E-mail address: mrm5@cam.ac.uk (M.R. Mackley).

0017-9310/$ - see front matter © 2008 Elsevier Ltd. All rights reserved.
doi:10.1016/j.ijheatmasstransfer.2008.01.036

Nomenclature

A_{cap}	total capillary surface area (m^2)
A_{LM}	log mean area (m^2)
A_{MCF}	surface area of one face of an MCF (m^2)
$\langle d \rangle$	average capillary diameter (m)
h	heat transfer coefficient (W/m^2 K)
I	current (A)
k	thermal conductivity (W/m K)
l	MCF length (m)
n	number of capillaries
$Q_{electrical}$	electrical power (W)
$Q_{thermal}$	thermal power (W)
T_{fluid}	fluid temperature (K)
T_{metal}	metal temperature (K)
U_v	volume heat transfer coefficient (W/m^3 K)
$U_{overall}$	overall area heat transfer coefficient (W/m^2 K)
V	voltage (V)

Greek letters

δ	thickness (m)
ΔT_{lm}	log mean temperature difference (K)

Subscripts

Al	aluminium
fluid	fluid
i	measurement location
metal	metal
PE	polyethylene
tape	double sided tape

Non-dimensional group

Nu	Nusselt number

cycling of a solution of DNA and enzymes between different temperature regimes.

Fast and precise heating and cooling is also beneficial in many areas of chemical processing. Due to their small mass, microreactors have very rapid thermal cycling times, and therefore the ability to control secondary reactions and by-products by rapid cooling of a synthesised product after the reaction is complete, results in higher purities [15]. With the wide variety of possible applications that require a fast heat transfer response on the micro-scale, coupled with the typically laminar flow regime within the fluid flow of these heat exchangers, this area of microengineering presents exciting opportunities for the development of innovative materials and novel devices.

This paper is concerned with the transient heat exchange properties of a novel material termed microcapillary film (MCF). MCFs are a class of novel, extrusion-processed, polymer films containing an array of continuous, parallel, capillaries that run along the film's length [16,17]. The current embodiment of the MCF product contains 19 capillaries with a mean hydraulic diameter typically around 200 μm; manipulation of process conditions can, however, result in mean hydraulic diameters ranging between 30 and 500 μm. MCFs have been successfully manufactured from a range of different polymers; the polymer that was used for the MCFs in this study was a commercially available linear low-density polyethylene (LLDPE) manufactured by the Dow Chemical Company Inc. (Dowlex NG5056G). A cross-section of a typical MCF is shown in Fig. 1.

A previous paper [18] presented an investigation into the hydraulic and steady-state heat transfer performance of LLDPE MCFs. This study demonstrated that, despite the plastic construction of the MCF, volumetric heat transfer coefficients of order 35 MW/m^3 K could be attained using both sides of an MCF for heat transfer, and around 14 MW/m^3 K for single-sided MCF systems. Additionally, heat transfer in a variety of geometric configurations could be achieved due to the flexible nature of the MCF.

The first section of this paper presents an experimental investigation into the temperature profiles that develop along MCFs whilst performing heat transfer duties in a flow system. Water is pumped through an MCF wound onto a cartridge heater and the temperatures of the surface of the film are recorded in six different locations. Using results from an additional experimental study, presented in Appendix A, it is possible to relate the surface temperature of the MCF to the average temperature of the fluid flowing in the MCF's capillaries. Furthermore, thermal imaging is used to investigate the natural convective cooling of hot water as is it is pumped along a vertically orientated MCF. Volumetric heat transfer coefficients are calculated for each case to serve as a comparison with literature values [8].

The second section of this paper then presents two case studies where MCFs fabricated into heat transfer devices are evaluated. The first of these presents an example where the direction of heat transfer is from a heated metal plate into fluid flowing within the MCF, this providing a proof-of-principle for the cooling of electronic components, such as computer processors. The second example demonstrates the reverse scenario. A strongly exothermic reaction is carried out within an MCF microreactor and the direction of heat transfer is from the reacting mixture flowing within the MCF to the external environment. Thermal imaging was used in each of these two case studies, providing valuable insight into the nature of the heat transfer as well as providing quantitative information on thermal gradients and temperature distributions. All MCFs used in the experimental work in this paper contained capillaries of average diameter 203 μm and standard deviation of 6.9%.

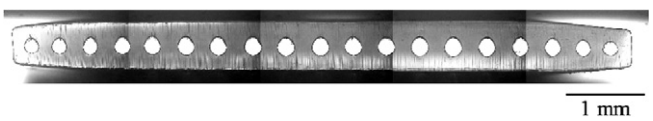

Fig. 1. Optical micrograph showing the cross-section of a typical MCF.

2. The experimental determination of temperature gradients within an MCF

2.1. Fluid heating

2.1.1. Equipment and experimental protocol

The equipment used to investigate the continuous heating of fluid in a length of MCF is shown in Fig. 2. A length of MCF was wrapped around a sleeved cartridge heater, with a layer of conductive paste (not shown in the diagram) to aid conduction between the two materials. The MCF was wound in such a manner that a small gap was left every two turns, exposing the surface of the heater sleeve. Water was pumped into the MCF at a controlled flowrate by means of a high pressure piston pump. The cartridge heater had an inbuilt *k*-type thermocouple that was used in the control loop to monitor the heater temperature. The surface temperature of the MCF was measured using additional *k*-type thermocouples

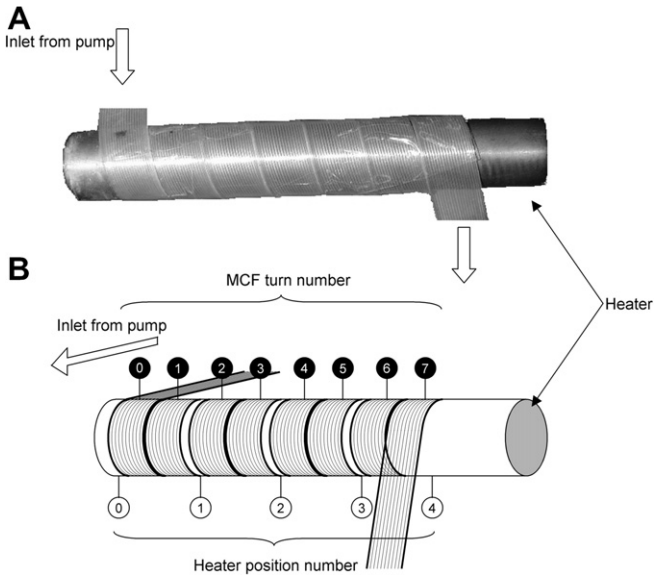

Fig. 2. (A) Photograph of MCF wrapped around a heater indicating direction of flow and (B) schematic diagram of the MCF wrapped around a heater showing the locations of the thermocouples on both the heater surface and the MCF surface.

placed in small-sized amounts of thermally conductive paste at seven locations, marked by white text on a black background in Fig. 2B. Further *k*-type thermocouples, placed in small-sized amounts of thermally conductive paste, were used to measure the surface temperature of the exposed brass sleeve at the five intermediate locations, shown in Fig. 2B by black text on a white background.

The volumetric flow-rate of water being pumped through the MCF was set to 5 ml/min and the heater set point temperature to 60 °C. After a few moments, once the system had reached a steady-state, the MCF surface temperature was measured in each of the seven locations and the temperature of the brass sleeve in each of the five locations. The experiment was then repeated with heater set point temperatures of 80, 100 and 110 °C.

2.1.2. Results and discussion

Experimental work, detailed in Appendix A, resulted in a correlation that allowed the surface temperature of the MCF to be related to the average temperature of the fluid flowing within the MCF capillaries. Plots of the MCF fluid temperature and brass sleeve surface temperature as a function of position for different heater set-point temperatures are shown in Fig. 3. Error bars in these plots have been set to ±2.2 °C since this is the standard uncertainty associated with a *k*-type thermocouple [19].

The fluid velocity in the capillaries at a volumetric flow-rate of 5 ml/min is 14 cm/s, resulting in a residence time of 0.23 s/turn and a total residence time of 1.6 s. It can be seen from the plot in Fig. 3A that the fluid within each capillary very rapidly approaches the temperature of the heater sleeve with the exit temperature of the fluid being within a few degrees Celsius of the heater temperature for heater set-points of 60, 80 and 100 °C. At 110 °C, the fluid exit temperature was about 100 °C indicating that the water had started to boil in the heat exchanger.

The trend of heater sleeve temperature as a function of position, shown in Fig. 3B, demonstrates that there is a significant temperature gradient along the heater whilst fluid flow is present in the MCF. Under no-flow conditions within the MCF, this gradient disappeared and the heater sleeve was uniformly 6 °C less than the heater set point temperature; this 6 °C difference was attributed to a calibration difference between the inbuilt heater thermocouple and those used to measure the surface temperature. It can be seen, therefore, that the cooling effect of the fluid flowing within the MCF on the brass is significant; over the first quarter of the heater sleeve length, its surface temperature is reduced by up to one-third of its no-flow temperature. The heater sleeve temperature increased steadily over the middle section of the casing before reaching a temperature within 2 °C of the no-flow temperature in the final third of its length.

The heat transfer coefficient based on the internal volume of the capillary array was calculated between each heating location. In order to do this, firstly the thermal power transferred to the fluid within a section of MCF was calculated, using the following equation:

$$Q_{\text{thermal}} = \dot{m} C_p (T_{\text{fluid},i} - T_{\text{fluid},i+1}) \tag{1}$$

In this equation, Q_{thermal} represents the thermal power, $\dot{m}$ the mass flow-rate of water, C_p the specific heat capacity of the water. The temperatures $T_{\text{fluid},i}$ and $T_{\text{fluid},i+1}$ represent the temperatures of the fluid within the MCF at a measurement location i, as shown by Fig. 2B. The fluid temperature at each location was calculated from the measured MCF surface temperature using the correlation outlined in Appendix A.

The overall heat transfer coefficient for the MCF heat exchanger based on internal volume, U_v, can be calculated between each measurement location using standard formulae [20]; this is shown in the following equation:

$$U_v = \frac{4Q_{\text{thermal}}}{n\pi\langle d\rangle^2 l \Delta T_{\text{lm}}} \tag{2}$$

In this equation, $\langle d\rangle$ is the average diameter of a capillary within the capillary array in the MCF, n is the total number of capillaries and l is the length of the MCF heat exchanger. The log mean temperature difference, ΔT_{lm}, is defined as shown in Eq. (3). Here, the definitions of $T_{\text{fluid},i}$ and $T_{\text{fluid},i+1}$are the same as those in Eq. (1) and $T_{\text{metal},i}$ and $T_{\text{metal},i+1}$ represent the heater temperature that would be found at each location where the fluid temperature is measured. These heater temperatures were calculated by linear interpolation of the measured heater temperatures under the assumption that the fluid measurement locations fall at one-quarter and three-quarters of the distance between each heater measurement point:

$$\Delta T_{\text{lm}} = \frac{(T_{\text{metal},i+1} - T_{\text{fluid},i+1}) - (T_{\text{metal},i} - T_{\text{fluid},i})}{\ln\left(\frac{(T_{\text{metal},i+1} - T_{\text{fluid},i+1})}{(T_{\text{metal},i} - T_{\text{fluid},i})}\right)} \tag{3}$$

Naturally convective heat losses from the surface of the MCF were calculated assuming a heat transfer coefficient of 5 W/m^2 K and found to be insignificant compared to the heat gain from the heater. Contact resistance between the heater and the MCF was neglected since generous quantities of thermal paste were used at the interface. A plot showing the heat transfer coefficient based on the total internal volume of the capillary array is shown in Fig. 4. It can be seen in this plot that there are potentially anomalous readings at positions 5 and 6. This has been attributed to the temperature of the MCF surface recorded at position 5 being slightly higher than would be expected given the trend of the remaining surface temperatures, as can be seen in Fig. 3A. This slightly higher reading also impacts the values of the heat transfer coefficients at position 6 and makes them slightly lower than would be expected given the data trend. The error bars for positions 5 and 6 have been adjusted to take this extra uncertainty into account, whereas the error bars for the remaining positions have again been set to represent an uncertainly of ±2.2 °C [19] in the measured fluid temperatures.

Despite the inaccuracy of the heat transfer coefficients at positions 5 and 6, it can be seen that the heat transfer coefficient calculated on a volumetric basis, values lie in the range 8 to 14 MW/m^3 K; the corresponding heat transfer coefficients calculated on

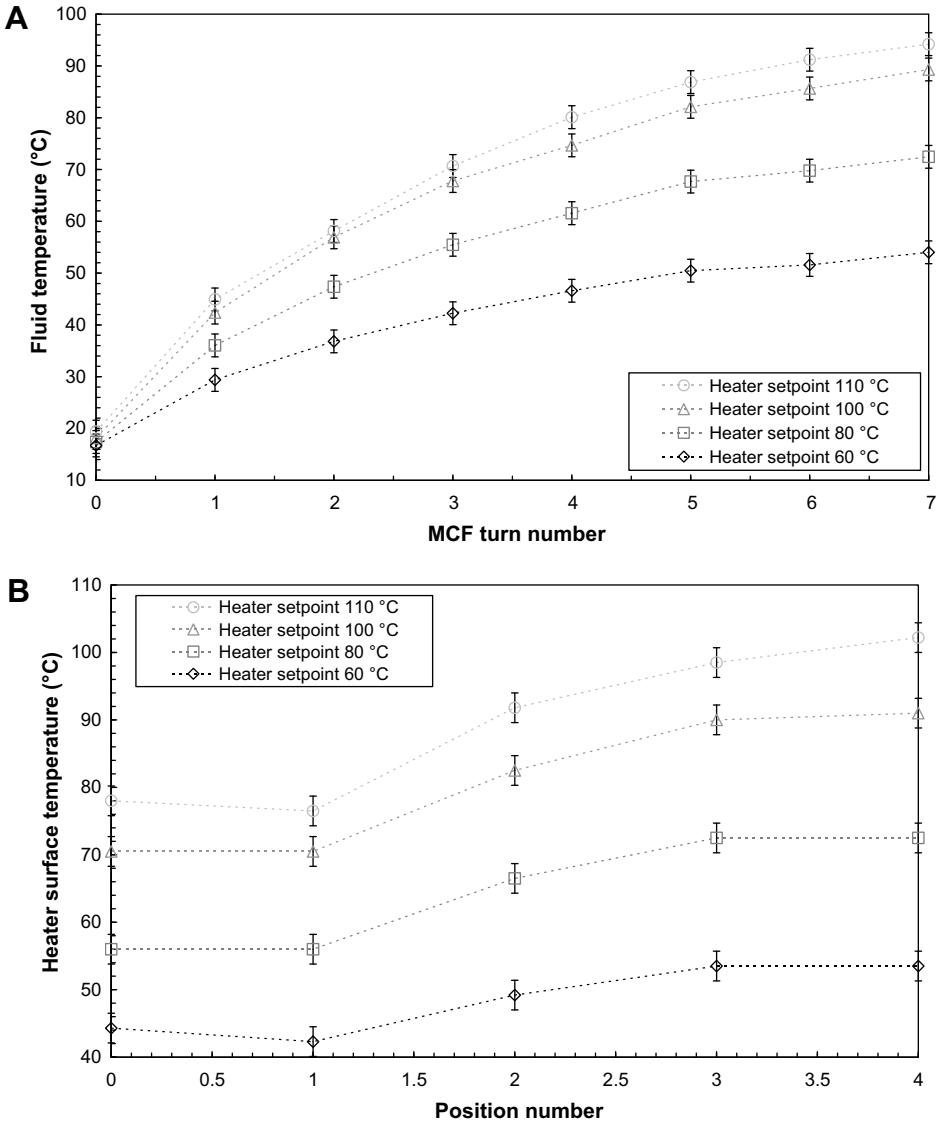

Fig. 3. (A) Plot of fluid temperature as a function of length along MCF for increasing heater set point temperatures. (B) Plot of heater surface temperature as a function of position for increasing heater setpoint temperatures. Lines between data points are intended as a visual guide only.

an area basis lie between 400 and 800 W/m^2 K. These values are comparable with values reported for a single-sided MCF heat exchanger [18].

2.2. Fluid cooling

2.2.1. Equipment and experimental protocol

This section of the case study presents experimental results of the cooling of fluid within an MCF, orientated vertically, under conditions of natural convection in free air. These results are intended to act as a baseline from which the effects of forced convective cooling could be investigated. A schematic diagram of the experimental equipment is shown in Fig. 5.

The heater set-point temperature was initially set to 50 °C. Water was pumped into the MCF using the high pressure piston pump outlined in the previous section, at a volumetric flow-rate of 1 ml/min hence giving an average velocity within each capillary of around 2.8 cm/s. A thermal imaging camera (FLIR SC3000) was used to image the MCF in the vertical section every 2 cm in the range 5–15 cm from the point at which the MCF left the heater sleeve. This procedure was repeated for 10 °C increments in heater set-point temperature up to 100 °C.

2.2.2. Results and discussion

A typical thermal image and temperature profile of the MCF is shown in Fig. 6.

It can be seen from Fig. 6B that the profile recorded by the thermal imaging camera can differentiate between locations in the film that contain a capillary and locations in the film that do not, with each of the capillaries appearing to be around 5 °C hotter than the polymer matrix surrounding it. This elevated capillary temperature could either be physically realistic or it could be an artefact of anisotropic emissivity. The thermal imaging camera was set to an emissivity of 0.93, a value that had been experimentally proved to correlate well with polyethylene. However, since the capillary walls within the MCF are very thin, it could be possible that the local emissivity in the vicinity of a capillary could be a bulk average of that of polyethylene (0.93) and that of water (0.98); this average would be higher than the emissivity of polyethylene alone, and hence would return a locally hotter temperature. Use of the

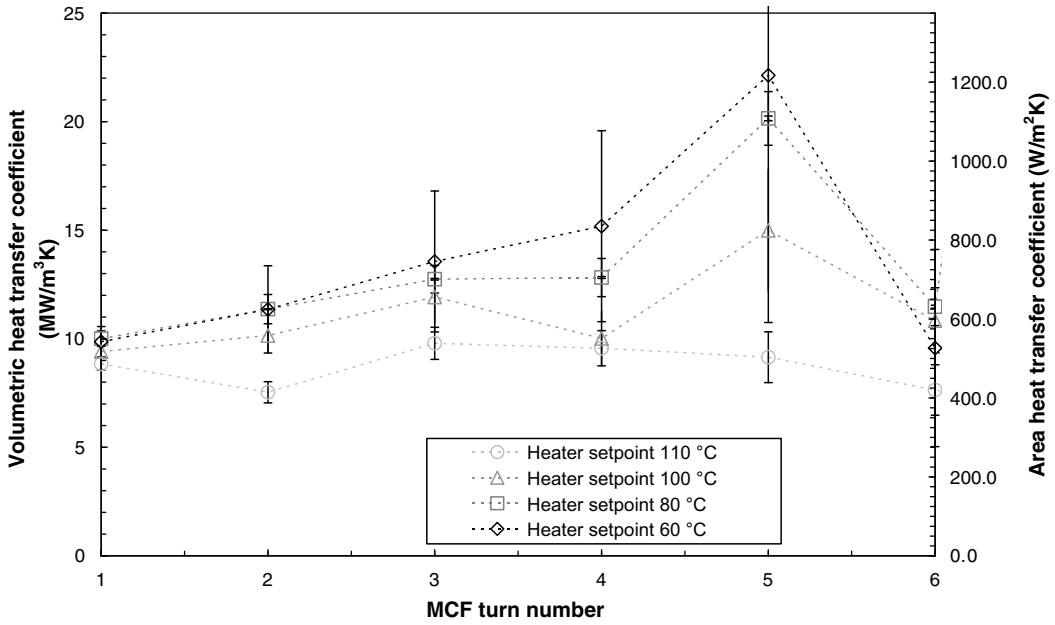

Fig. 4. Plot of heat transfer coefficients as a function of position along the heater for different heater set-point temperatures. The volumetric flow of fluid was 5 ml/min during all experiments and the lines between the data points are to assist visual clarity only.

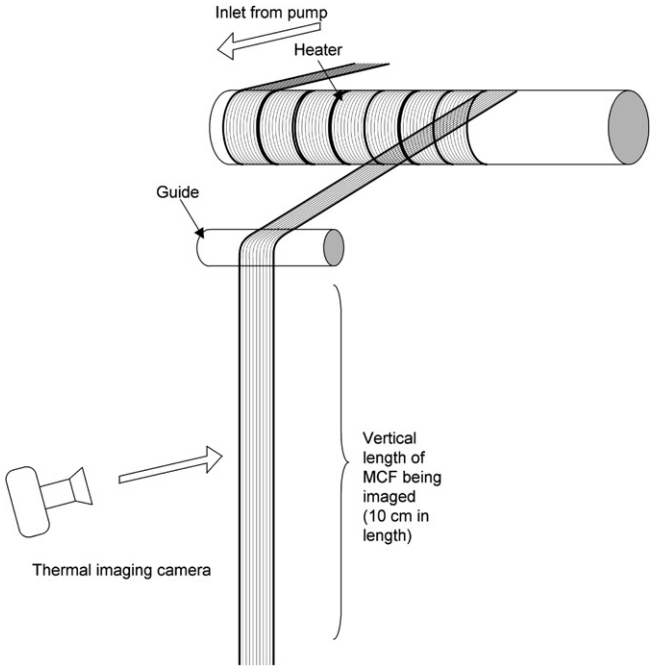

Fig. 5. Schematic diagram of the experimental apparatus used to investigate the cooling of fluid within an MCF using natural convection. The fluid is firstly heated in the MCF wrapped around the heater before being allowed to cool in the vertical section; a thermal imaging camera was used to map out the thermal profile of this section.

thermal imaging camera, therefore, to obtain accurate absolute temperature measurements must be therefore done with care.

Fig. 7A shows the variation in temperature as a function of distance along the MCF at different heater set-point temperatures. In this plot, each temperature point corresponds to the average of the maximum temperatures, each corresponding to the location of a capillary, that were recorded by the thermal imaging camera when set to an emissivity of 0.93. These data are re-plotted on semi-log axes in Fig. 7B to form a composite mastercurve. Each set of data, corresponding to a different heater set-point temperature, has been shifted in length such that the temperature profile of fluid with an MCF undergoing cooling by natural convection can be extrapolated to lengths longer than that was initially imaged.

The plot of Fig. 7B suggests that there are two regimes of heat transfer, each with subtly different heat transfer coefficients. Fig. 8 shows a plot of the calculated heat transfer coefficients based on both internal capillary volume and internal capillary area as a function of average temperature within the MCF. These values were calculated using Eqs. (1)–(3). The log mean temperature difference was based on the difference between the inlet and exit temperatures recorded by the thermal imaging camera and the measured ambient temperature, the area that was used was the total internal area of the capillaries and the difference between the inlet and exit temperatures multiplied by the heat capacity flowrate was used to calculate the thermal power. It is not clear from the plot shown in Fig. 8 whether the heat transfer coefficient is constant, or whether it changes as Fig. 7B suggests. Moreover, it is not clear that if a change exists, whether this could be attributed to subtle differences in experimental technique or a physical effect. Clearly, further experimental work is required to resolve this question. What is clear, however, is that the magnitude of these coefficients are both roughly a factor of 20 lower than their respective heating coefficients given in Fig. 4. This suggests that the efficiency of cooling the fluid within the MCF using natural convection is not very high. Error bars in this plot correspond to a temperature uncertainty of ±1 °C which was due to uncertainty within the thermal imaging.

3. Case study 1: heat transfer to the fluid flow – a prototype electronics heat exchanger

3.1. Equipment and experimental protocol

A schematic diagram of the experimental equipment used to investigate a prototype MCF electronics heat exchanger is shown in Fig. 9.

Cooling water was taken from the mains water supply and pressurised to roughly 5 barg using a small piston pump; the

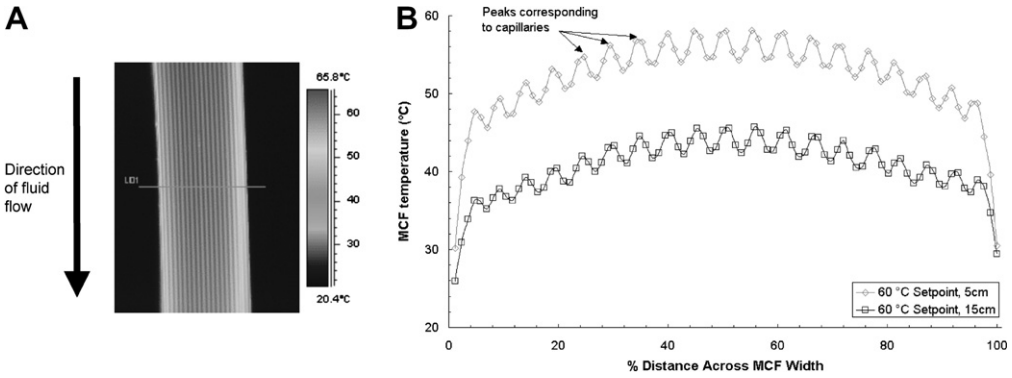

Fig. 6. (A) Typical thermal image of the vertically orientated MCF. The horizontal line on the image represents the locations where temperature data is recorded. (B) Typical plot of MCF temperature as a function of position across an MCF. These data were measured by the thermal imaging camera at a distance of 5 cm from the point where the MCF left the heating sleeve (open diamonds) and at a point 15 cm from where the MCF left the heating sleeve (open squares) for a heater set-point temperature of 60 °C. The emissivity was set to 0.93.

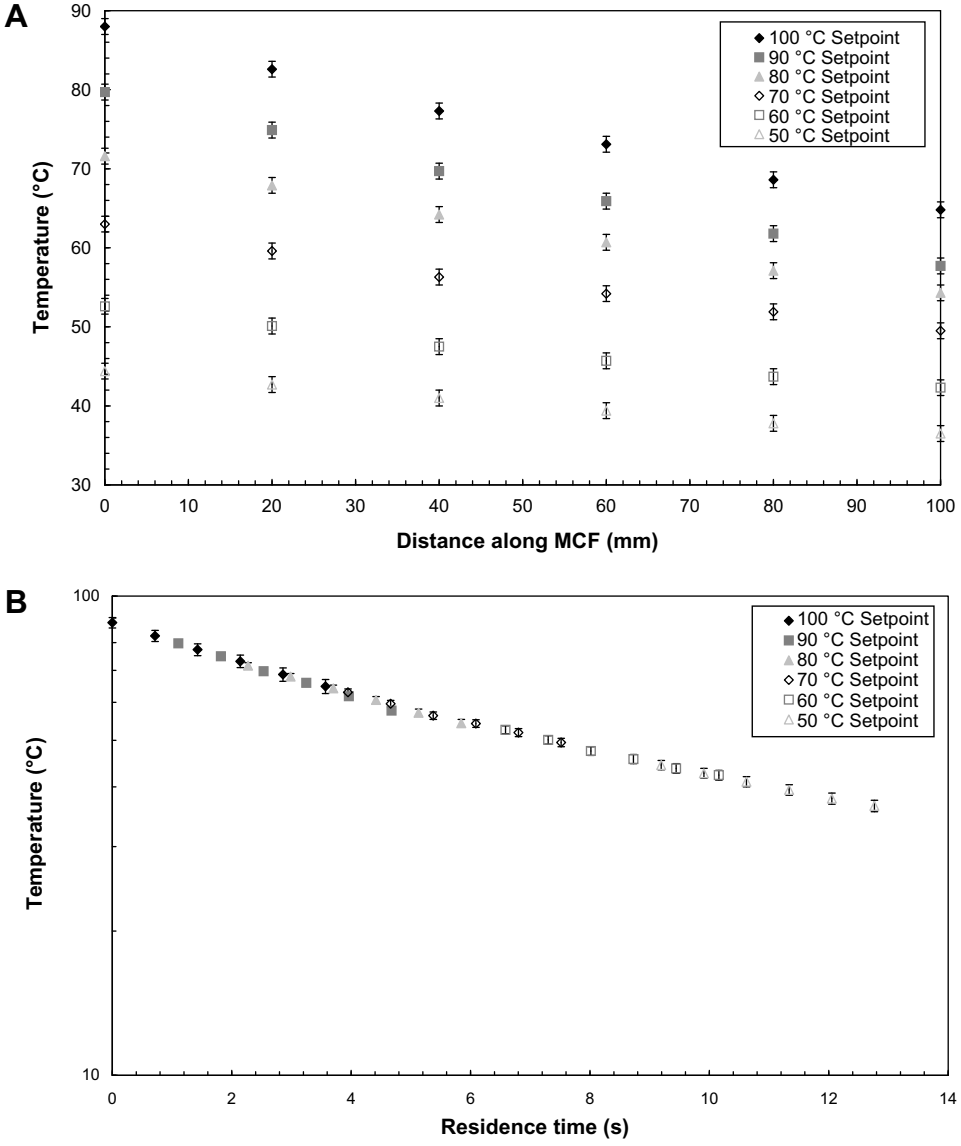

Fig. 7. (A) Plot of the average maximum temperatures as a function of distance along the MCF for different heater set-point temperatures. (B) Composite plot of the average maximum temperatures as a function of residence time in the MCF; the data for each heater set-point temperature has been shifted in length to produce a cooling mastercurve.

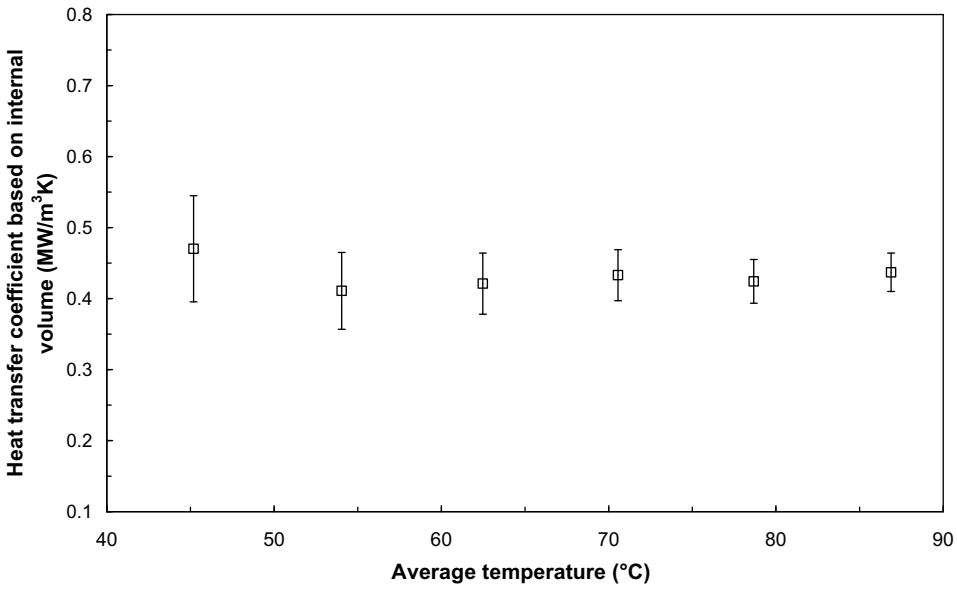

Fig. 8. Plot of the heat transfer coefficients based internal volume as a function of average temperature within the MCF under naturally convective cooling conditions.

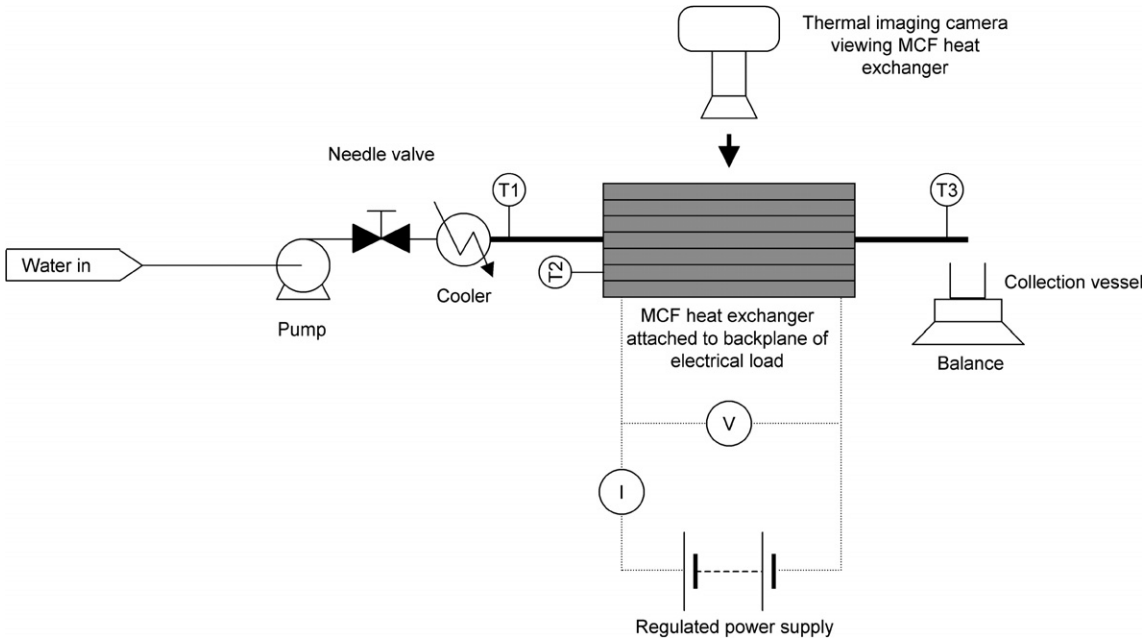

Fig. 9. Schematic diagram of the equipment used to simulate heat exchange from electronic components showing the cooling water supply, MCF heat exchanger and electrically heated thermal load.

volumetric flow-rate of water exiting the pump was controlled by means of a manual needle valve. Prior to entering the MCF heat exchanger, the water passed through a coiled copper tube that was immersed in an agitated bath containing a mixture of ice and water. The temperature of the fluid exiting the coiled copper tube was measured by means a *k*-type thermocouple that had been mounted within a Swagelock® union with epoxy resin such that it was in contact with the cold water flow. Connected to the outlet side of the Swagelock® union was a bundle of seven parallel LLDPE MCFs that had been glued in place to allow the water to flow into the capillaries. A thick layer of thermal insulation had been adhered to the MCF bundle between the union exit and the active surface of the heat exchanger to minimise heat transfer from the environment to the fluid flow. The seven MCFs were adhered to the back of a small aluminium plate using a very thin double-sided tape adhesive; this plate could be heated and these seven MCFs constituted the working part of the heat exchanger. A photograph of this exchanger is shown in Fig. 10A. The MCF bundle leading away from the active heat exchange surface was again wrapped in a thick layer of insulation until it was terminated in another Swagelock® union fitted with an embedded *k*-type thermocouple. Water leaving this union was collected in a collection vessel on a top-pan balance such that the time averaged water flow-rate could be accurately calculated. The thermal power removed by the heat exchanger, $Q_{thermal}$, could be calculated in a standard way [20], as shown in Eq. (1).

Three high-power 2.2 Ω resistors were mounted to the reverse face of the aluminium plate which the MCFs were attached to.

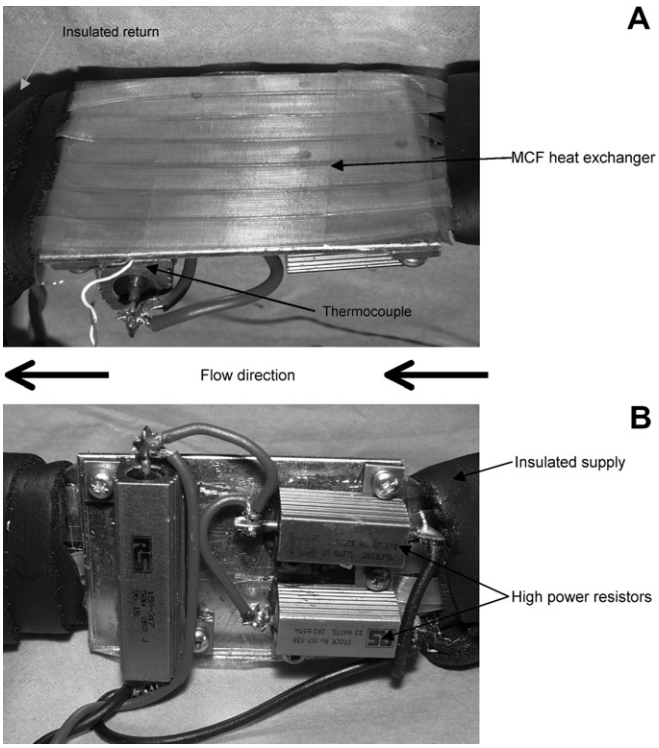

Fig. 10. Photographs of the experimental equipment used to simulate heat exchange from electronic components. (A) Front view showing placement of high power resistors and (B) back view showing the MCF heat exchanger adhered to the aluminium plate and the placement of one of the thermocouples.

These resistors were connected together in parallel thus presenting a resistive load of 0.73 Ω to the power supply. It was assumed that the dissipation from each resistor would be similar, within the manufacturing tolerance of the components, therefore the temperature of the hottest part of the heated plate was measured by a *k*-type thermocouple that was attached to the underside of one of the resistors. Heat transfer paste was liberally smeared on the surfaces of both the resistors and the aluminium plate to aid heat transfer. A photograph of the assembly is shown in Fig. 10B. The resistors were connected to a variable power supply that was capable of supplying loads up to 50 W at high current. Voltage and current measurement was built in to the power supply, providing a convenient way to measure the electrical power supplied to the resistive load, $Q_{electrical}$, as shown in the following equation:

$$Q_{electrical} = VI \tag{4}$$

A thermal imaging camera (FLIR SC3000) was mounted on a XYZ table in such a way that the infra-red emission from the active part of the MCF heat exchanger could be examined. The camera's field of view was such that roughly one-ninth of the active surface area could be viewed at any one time. An image of the entire active surface was obtained by waiting until a steady-state heat transfer situation had been reached and then by traversing the camera on the XYZ stand by pre-calculated amounts, taking a picture in an appropriate location. The resulting nine images were then combined to create the final image.

The protocol for running the experiments was as follows. Firstly, the water flow was set to 30 ml/min without power supplied to the resistive load on the heat exchanger. The temperature of the water entering and leaving the active part of the heat exchanger was measured at steady-state such that the thermal load under background conditions could be calculated. A steady-state was assumed to have been reached when the temperature of the aluminium plate, recorded by the thermocouple mounted under one of the three resistors, no longer changed. At steady-state, nine thermal images of the exchanger were taken. Keeping the water flow constant, the power supply was turned on and varied such that the power applied to the resistive load spanned five levels between 11 W (electrical) and about 50 W (electrical). At each different power setting, the temperature of the water entering and leaving the heat exchanger was recorded once a steady-state had been achieved, and a composite thermal image acquired. Additionally, voltage and current measurements were recorded such that the electrical power applied could be accurately calculated. This protocol was repeated for water flow-rates of 60 and 120 ml/min.

3.1.1. Results and discussion

A plot of the thermal power removed by the MCF heat exchanger as a function of the resistive load's electrical power for different volumetric flow-rates of water is shown in Fig. 11. Marked on this

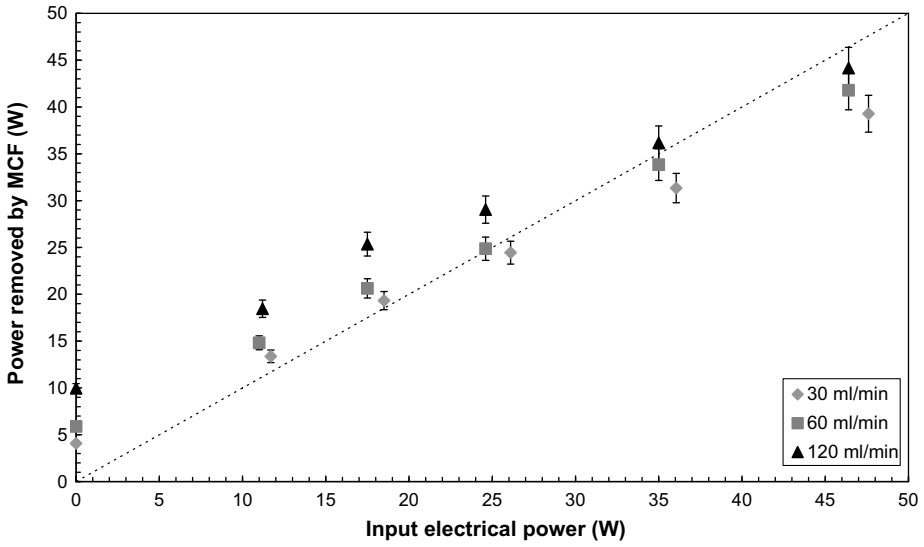

Fig. 11. Plot of thermal power removed by the MCF heat exchanger as a function of input electrical power for increasing MCF fluid flow-rates. The black dotted line represents $y = x$, where the power removed and the input power are the same.

diagram is the locus of points corresponding to $y = x$ which is the point where the thermal power extracted by the MCF heat exchanger matches the electrical power supplied to the resistive load.

There are several features shown in this plot. Firstly, there is always thermal power extracted by the heat exchanger, even when the electrical power supplied to the resistive load is zero. This is due to heat transfer from the ambient surroundings to the plate containing the resistors and the heat exchanger coupled with the fact that the water temperature entering the active part of the heat exchanger was close to freezing point. It can also be seen on this plot that there is a trend of increasing thermal power extraction with applied electrical load. This suggests that at no point in any of the experiments did the heat exchanger reach the limit of its operation, with the water becoming 'saturated' with heat. A further observation that supports this conclusion is that successive doubling of the volumetric flow-rate of water through the heat exchanger from 30–60 to 120 ml/min has little effect on the thermal power extracted.

In terms of the effectiveness of the MCF heat exchanger, between zero and roughly 17 W of electrical power, the heat exchanger is typically removing more thermal power than applied electrical power as a result of the influence of the ambient conditions. Over 17 W, the thermal power extracted from the resistive load is less than the electrical power supplied. This is not surprising, since not only are there a series of thermal resistances between the heat source and the MCF heat exchanger but, as can be seen in the photograph in Fig. 10B, the resistors are large and have an outer casing designed to convect heat away from the surface.

The overall heat transfer coefficient was calculated on the basis of the total internal area of the capillaries, using Eqs. (1)–(3). These data are plotted in Fig. 12b. The typical values of the overall heat transfer coefficient are between three and four times lower than those previously reported [18] for a heat transfer set-up where only one side of the MCF is in contact with a heated surface. This is likely to be due to the quality of the adhesion between the MCF surface and the surface of the plate and the subsequent increase in heat transfer resistance. The interfacial heat transfer coefficient, h_{contact}, can be calculated using the equation shown in the equation:

$$h_{\text{contact}} = \frac{1}{A_{\text{MCF}}\left(\frac{1}{A_{\text{cap}}U_{\text{total}}} - \frac{\delta_{\text{Al}}}{A_{\text{MCF}}k_{\text{Al}}} - \frac{\delta_{\text{tape}}}{A_{\text{MCF}}k_{\text{tape}}} - \frac{\delta_{\text{PE}}}{A_{\text{LM}}k_{\text{PE}}} - \frac{\langle d\rangle}{Nuk_{\text{fluid}}A_{\text{cap}}}\right)} \quad (5)$$

In this equation, U_{total} represents the overall heat transfer coefficient; the thicknesses of the aluminium plate, double-sided tape and the walls of the MCF are represented by δ_{Al}, δ_{tape}, and δ_{PE}, respectively, and their thermal conductivities by k_{Al}, k_{tape}, and k_{PE}. The heat transfer areas A_{MCF} and A_{cap}, respectively, represent the surface area of one of the MCF faces attached to the aluminium plate and total internal surface area of the capillaries within one MCF attached to the aluminium plate. A_{LM} represents the log mean of these two areas. The heat transfer from the walls of the polyethylene MCF to the fluid flowing within the capillaries is assumed to be analogous to convective heat transfer to a laminar fluid flow within a tube having a constant surface temperature. The final term in the denominator of Eq. (4) represents an estimate of this convective heat transfer coefficient based on a Nusselt number, Nu, of 3.656 [20]. If a typical overall heat transfer coefficient that was calculated from this experiment, 150 W/m^2 K, is used to calculate the interfacial heat transfer coefficient, it is clear that the contact resistance dominates this heat transfer problem; the interfacial heat transfer coefficient is almost a factor of 10 lower than the next smallest value. Interestingly, if a typical heat transfer coefficient from the fluid heating experiment in Section 2.1 is used, roughly 800 W/m^2 K, it demonstrates that the use of heat transfer paste greatly improves the situation as the limiting heat transfer resistance is that of the polyethylene walls of the MCF rather than that of the contact. Full details are given in Table 1.

The ability to image the operation of the MCF heat exchanger in the infrared spectrum is a powerful method of assessing the exact operation of the heat exchanger under different experimental conditions. Fig. 13 shows two images of the MCF heat exchanger in operation with an applied electrical load of 24 W; Fig. 13A is at a water flow of 30 ml/min and Fig. 13B is at 60 ml/min. The dotted lines in the figure denote the edges of one the strips of MCF.

These images provide insight into the how quickly the fluid within the MCFs heats up as a function of flow-rate and position along the heated surface. In general, the fluid contained in the

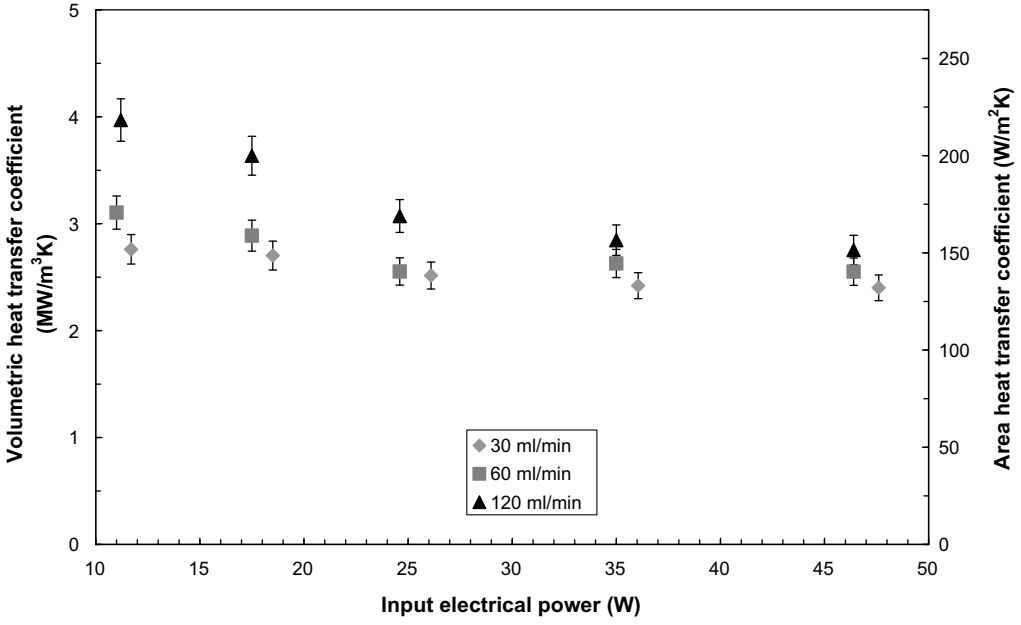

Fig. 12. Plot of heat transfer coefficient calculated on a volumetric basis as a function of input electrical power for different volumetric flow-rates of water through the MCF.

Table 1
Individual heat transfer coefficients for MCF heat exchanger calculated for two different overall heat transfer coefficients

	Individual heat transfer coefficients for $U_{overall}$ = 150 W/m^2 K (W/m^2 K)	Individual heat transfer coefficients for $U_{overall}$ = 800 W/m^2 K (W/m^2 K)
Conductive HTC for aluminium plate	103,000	103,000
Contact HTC	280	24,800
Conductive HTC for double-sided tape	5000	5000
Conductive HTC for polyethylene	1590	1590
Convective HTC to fluid flow	10,600	10,600

MCF capillaries closest to the edges tends to heat up quickest. This is expected since the MCF manufacturing process almost always results in slightly smaller diameter capillaries at each edge [21], hence the fluid velocity in these capillaries will be smaller for a constant pressure drop across the entire capillary array. The majority of the fluid, however, contained within the bulk of the capillaries tends not to heat up to the same extent. This observation suggests that the fluid is capable of extracting more thermal energy hence longer lengths of MCF in a heat exchanger would still perform useful heat transfer.

4. Case study 2: heat transfer from the fluid flow – cooling of an exothermic reaction

4.1. Introduction

MCFs are flexible, continuous in length, and can be shaped in various configurations in order to match the needs of different chemical reactions. Previous work has been carried out on the use of a compact MCF microreactor for liquid phase reactions [22] where a single film of typically 5–40 m in length was rolled up and heat pressed to form a solid disc reactor. These devices are designed to carry out slow reactions in continuous flow, such as organic synthesis, with residence times of up to 2 h. The flow-rates in these cases were very low, typically between 0.1 and 1 ml/min, hence fast and efficient heat transfer is not important.

In fast reactions, where the heat transfer needs to be optimised, either the cooling of an exothermic reaction, the heating of an endothermic reaction or also for accurate temperature control in general, MCF structures that maximise heat transfer area are beneficial. This case study is concerned with a microreactor which consists of a mixing cell that allows two MCF feed lines to be combined with the combined flow entering an MCF that is either tightly coiled around a metal rod or kept straight. A simple neutralisation reaction was carried out inside the MCFs and the heat produced was monitored with a thermal imaging camera (FLIR SC3000).

4.2. Equipment and experimental protocol

The first part of the microreactor is a customised MCF mixing cell. This unit was made up of three MCFs, laminated together with two blank sealing films, with holes connecting the central capillaries. Fig. 14 shows a schematic diagram and a photograph of the mixing cell. The device enables two feed lines (marked in the diagram with A and B) to be fed into one MCF inside a small unit without the use of external connectors and fittings.

The mixing cell was manufactured in five steps. Firstly, the entrances of three MCFs were heat sealed by melting the final few millimetres of each film. Then these three films were laminated together at a controlled temperature close to the melting point of the plastic for 5 min using a heated press; for the LLDPE films

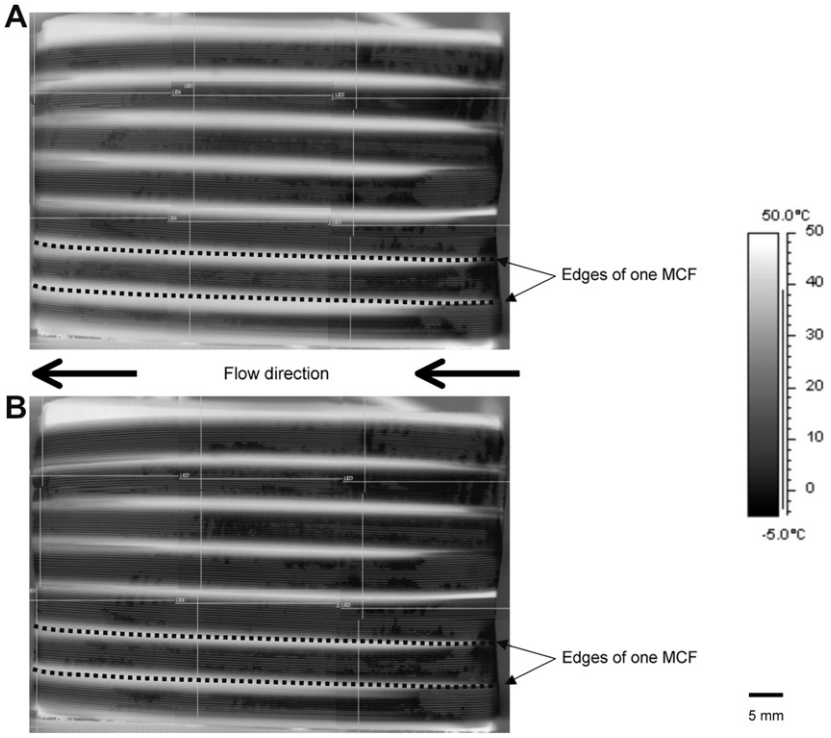

Fig. 13. Compound thermal images of the MCF heat exchanger at (A) 30 ml/min and (B) 60 ml/min with an electrical load of 24 W. The flow direction in each image is right to left and the dotted lines represent the edges of one of the MCFs within the heat exchanger. The emissivity was set to 0.93.

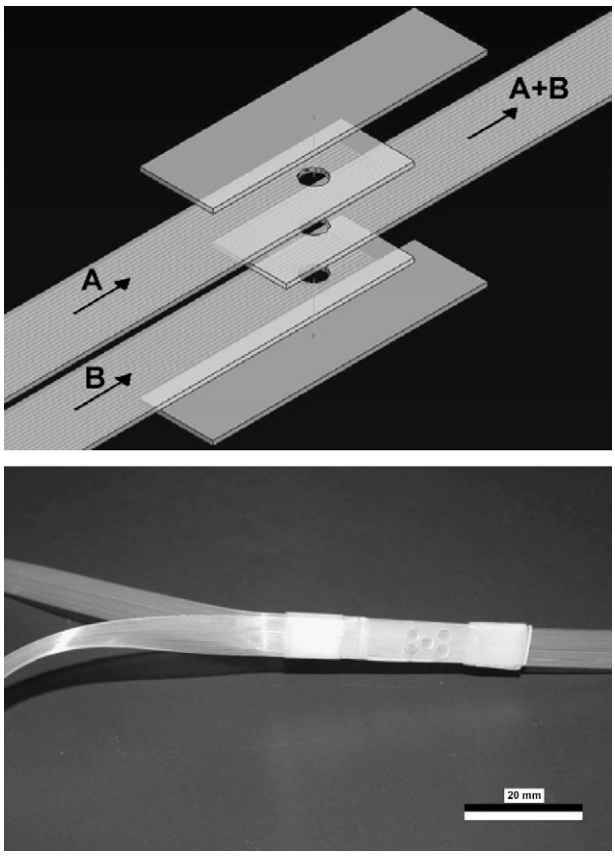

Fig. 14. Diagram and photograph of an MCF mixing cell.

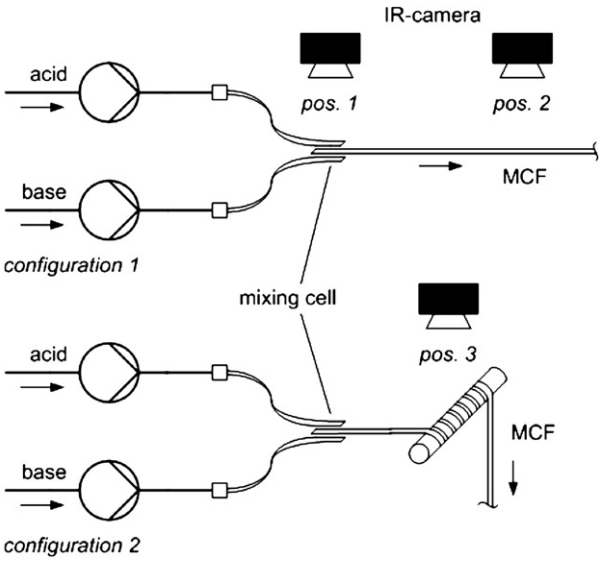

Fig. 15. Schematic diagram of the experimental set-up of an acid–base neutralisation, carried out inside an MCF and monitored with a thermal imaging camera.

used in these experiments, the temperature was set to 116 °C. This process allowed the flat surfaces of the MCFs to form a solid, gapless, joint without melting or deforming the capillaries inside the films. After cooling down, either one or a number of holes were punched into the unit perpendicular to the capillaries, such that up to 10 of the central capillaries in the three MCF layers could be connected together. The fourth step consisted of a second heat treatment step: blank, capillary-free, films were layered on the top and bottom of the mixing holes, using the same process conditions as in the first laminating step, such that they were sealed. In a final step, a short length of heat shrink tubing, made from a polyolefin, was shrunk over the whole unit to act as a further seal.

This device represents a compact method for joining together two fluid streams and feeding them into one MCF. This not only minimises the fluidic pathway between the mixing point of the two streams and the entry into the MCF but also uses a minimal amount of material.

Fig. 15 shows a schematic diagram of two experimental configurations used to investigate a fast exothermic liquid phase reaction performed inside MCFs in continuous flow mode.

For this set of experiments, two high pressure piston pumps were used to supply a constant flow of acid and base into the microreactor consisting of two MCF feed lines, an MCF mixing cell and a main MCF reactor. The two configurations shown in Fig. 15 were used to investigate cooling solely due to natural convection (configuration 1) and cooling by conduction to a solid cylindrical object at ambient temperature (configuration 2). The thermal imaging camera was used to image the heat produced during an exothermic acid–base reaction at three different points in the system; at the mixing cell (position 1), at a point in the straight MCF section (position 2) and at a point in the coiled section (position 3). The latter two of these positions were downstream from the point of mixing (see Fig. 15).

To test this microreactor, a simple acid–base neutralisation between acetic acid and triethylamine was chosen, which has very fast kinetics and produces enough heat to be monitored with a thermal imaging camera. Fig. 16 shows the acid-to-base proton-transfer of this system.

A solution of both acid and base in 50% acetonitrile was chosen. The total flow-rate through the microreactor was set between 0.1 and 4 ml/min, with an equal ratio between acid and base phases (0.05–2 ml/min acid/base flow-rate). These conditions produced good results, heating up the fluid phase inside the capillaries up to 60 °C, without working with too concentrated a system.

The experiments were conducted in short runs. From the point of switching on both pumps, it took the system anywhere between a few seconds to several minutes to reach steady-state. Once images and data from steady-state conditions were collected, the pumps were turned off which lead to the cessation of flow within the capillaries within a few seconds and a cooling down of the microreactor a few seconds after that. Movie sequences with the thermal imaging camera were taken to monitor the transition states, and still images were taken at steady-state.

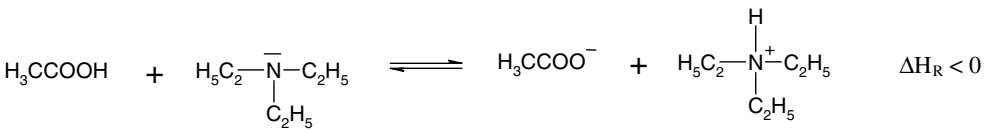

Fig. 16. Exothermic acid–base neutralisation: acetic acid + triethylamine.

4.3. Results and discussion

Fig. 17 shows four images taken at steady-state conditions at three different positions of the microreactor. Fig. 17A shows the MCF mixing cell at 0.1 ml/min (at camera position 1), Fig. 17B the MCF mixing cell at 4 ml/min (at camera position 1). Fig. 17C shows the straight MCF 120 mm downstream from the mixing point (at camera position 2), and Fig. 17D shows the coiled MCF, directly after the mixing point (at camera position 3). The light open rectangle in the lower part of the first two images indicates the mixing point where the acid and base feed lines join. From this point downstream, the neutralisation reaction takes place leading to the liquid inside the capillaries being heated up. White arrows on the images indicate the flow direction, and a legend at the side represents the monitored temperature range.

Average and maximum temperatures were calculated at different points of these images for different flow-rates using software that was supplied with the thermal imaging camera. Temperature profiles could be taken at the mixing point (within the light rectangle) and across a line over the central active capillaries of the MCF a few millimetres downstream from the mixing cell, for images a and b. In the same fashion, average and maximum temperatures were determined across the active channels of a straight MCF in image c and across the active channels at five different positions along a coiled section in image d. In the latter case, the first of these five temperature profiles was taken upstream from where the MCF contacts the steel rod, the second up to the third profiles were taken at the beginning of coils 1–4 (see Fig. 17).

Fig. 18 shows temperature profiles for these sections as a function of flow-rate. Fig. 18A shows the average and maximum temperatures at the mixing point and at the MCF a few millimetres downstream (camera position 1), Fig. 18B the average and maximum temperatures at the central active capillaries and the average temperature of the whole cross-section of a straight MCF (camera position 2) Fig. 18C shows the average temperature profiles at five different positions along a coiled MCF section (camera position 3).

Temperature profiles at the mixing cell (Fig. 18A) show a general upwards trend with increasing flow-rate. The temperature in the main reactor MCF is roughly 10 K higher than at the mixing point, except for very low flow-rates (0.1 ml/min). The crossover of these two lines in the first plot can be explained by the fact that, at low flow-rates, most of the reaction is occurring in the mixing cell. Due to the rapid heat transfer out of the system, the fluid bulk has already cooled down significantly by the time it exits the mixing cell and flows down the reactor MCF. For flow-rates between 0.5 and 4 ml/min, the temperatures measured in the main film are higher than at the mixing point. This results from the higher convective heat and mass transport along the channel due to the increased flow velocities, which leads to the reaction and heat transfer across the polymer walls taking place further downstream.

Most of the temperature profiles further downstream in the MCF, plotted in Fig. 18B and C show a steep increase in temperature at low flow-rates and a slow increase at high flow-rates. The profiles taken at the 2nd, 3rd and 4th coil, shown in Fig. 18C, demonstrate a trend of decreasing temperature with turn number; this is due to the cooling effect that the metal rod has on the flow inside the capillaries. This cooling effect could be significantly increased by installing an active cooling system, such as a pipe with a chilled liquid flow inside, instead of just having a solid object. This set of experiments shows, that a highly exothermic reaction can be carried out and cooled efficiently in a small microreactor system using MCFs.

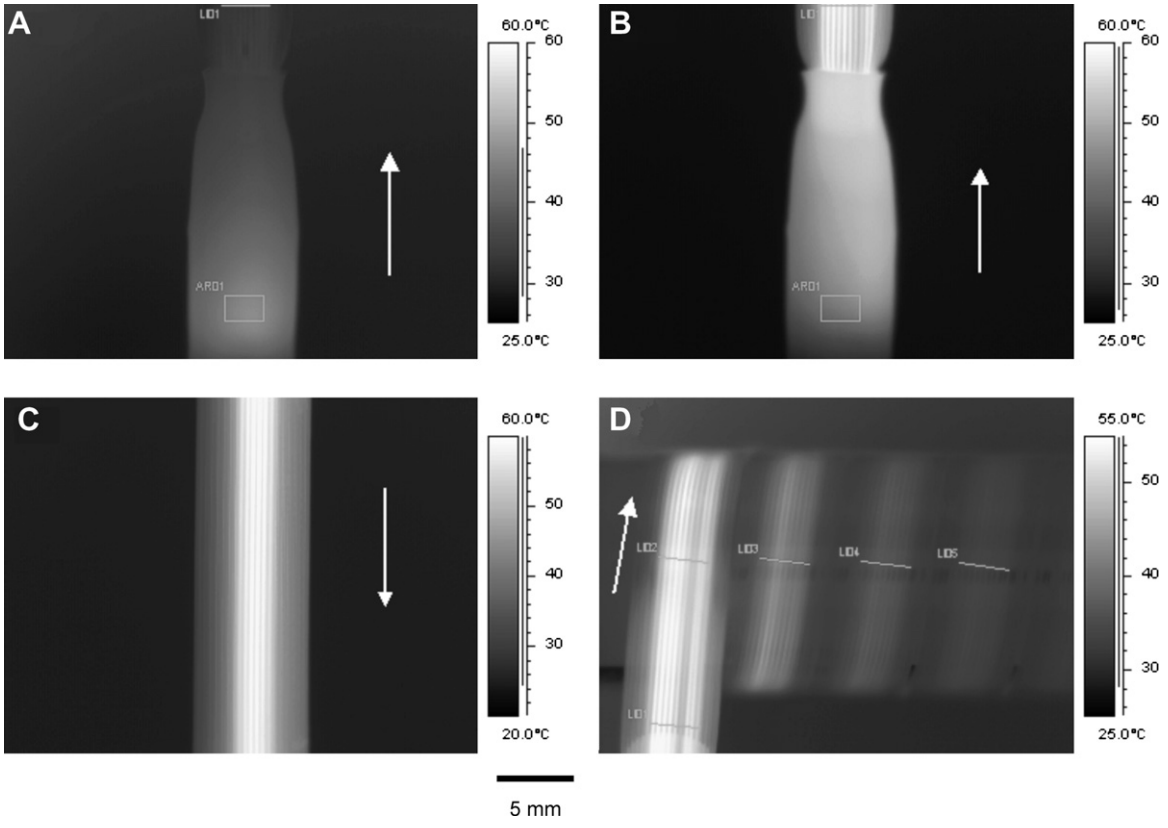

Fig. 17. Thermal images of the MCF microreactor at different positions: (A) camera position 1 at 0.1 ml/min, (B) camera position 1 at 4 ml/min, (C) camera position 2 at 4 ml/min and (D) camera position 3 at 4 ml/min, arrows indicating the direction of flow.

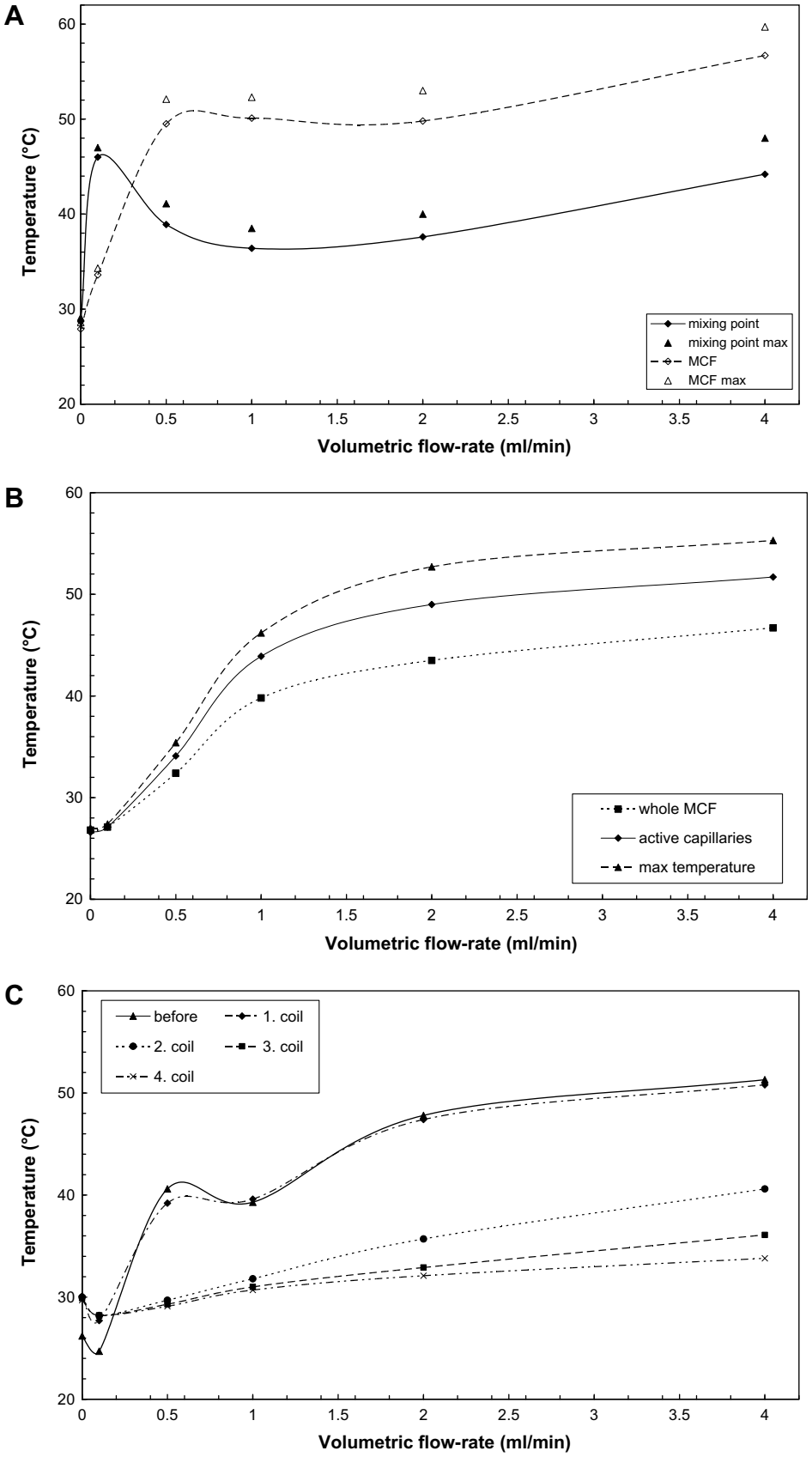

Fig. 18. Temperature profiles as a function of volumetric flow-rate through the microreactor, measured at three different camera positions: (A) at the mixing cell (position 1), (B) at a straight MCF section (position 2) and (C) at a coiled MCF section.

5. Conclusions

This paper has presented an experimental investigation of the development of temperature profiles along MCFs when used for heat exchange in flow systems along with two case studies where MCFs have been successfully used as micro heat exchange devices. Despite their plastic construction, the experiments presented in this paper have shown that these devices are effective heat exchangers that can remove heat either from a heated surface (in the case of microelectronics cooling) or from a highly exothermic chemical reaction. Heat transfer coefficients based on internal volume have been typically in the region between 8 and 14 MW/m^3 K (400–800 W/m^2 K in terms of internal capillary area) when the MCF has been in direct contact with the heated surface, or around 0.43 MW/m^3 K (around 21.5 W/m^2 K) for naturally convective cases. The figures for direct contact are consistent with previous research [18] for a single-sided MCF heat exchanger. Experimental data has also shown that the quality of adhesion between the heat exchanger and a surface is an important factor in determining overall heat transfer performance and that in a practical design, great care must be used in joining together these surfaces.

Novel features of MCF heat exchange devices include their long length and their flexibility; these features have allowed innovative heat exchange configurations to be tested in each application area. The ability to wrap a thin-film heat exchanger over a non-uniform surface could have interesting application in space-critical heat removal.

Thermal imaging has been used to characterise and quantify the operation of the MCF heat exchangers. This has proved to be very useful in providing detailed insight into the temperature profiles within operational devices. However, care must be taken when making absolute temperature measurements with such an instrument though, since slight changes in surface emissivity can lead to erroneous measurements.

Acknowledgements

The loan of the thermal imaging camera from the EPSRC engineering instrument pool along with the assistance of Peter Anthony is gratefully acknowledged. Funding from an EPSRC platform grant, Platform for Process Innovation, is also acknowledged. The authors would furthermore like to thank Professor Steven Ley and Dr. Ian Baxendale for the generous use of equipment in the Department of Chemistry, University of Cambridge which was employed to carry out continuous flow acid–base reactions within MCF microreactor units.

Appendix A. The relationship between surface and fluid temperatures within an MCF

A.1. Experimental method

The easiest temperature measurement to make on an MCF, in the absence of an instrument such as a thermal imaging camera, is surface temperature. It is desirable, therefore, to establish a correlation such that the external surface temperature of the MCF and the fluid temperature within the MCF can be related. A schematic diagram of the experimental equipment is shown in Fig. A1.

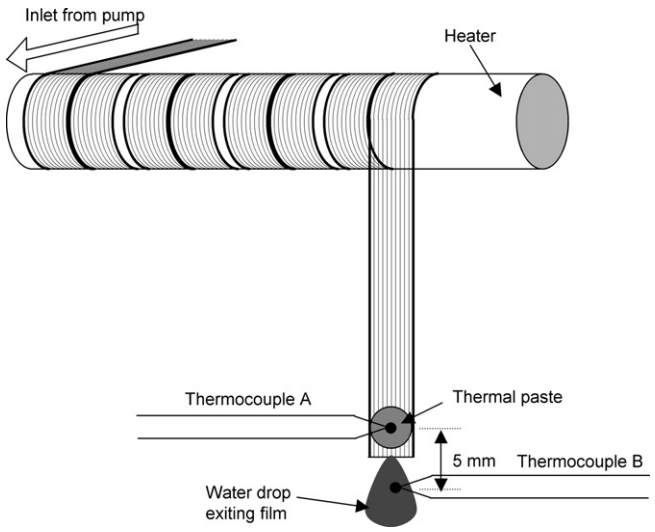

Fig. A1. Schematic diagram of the apparatus used to correlate the surface temperature of the MCF to the bucket temperature of the fluid flowing within the capillaries.

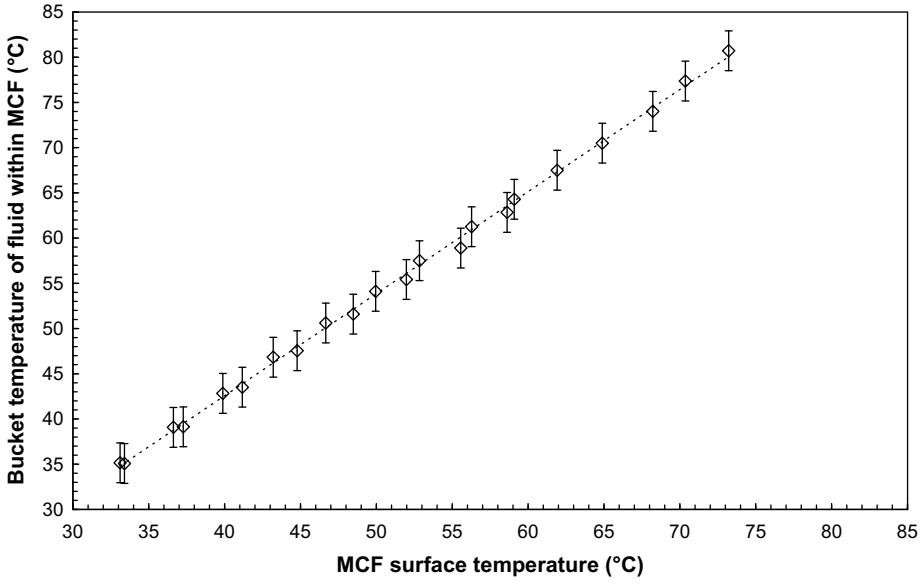

Fig. A2. Plot of the bucket temperature of the fluid exiting the MCF as a function of MCF surface temperature.

An MCF was wrapped around a sleeved cartridge heater seven times and a short section taken vertically downwards. A *k*-type thermocouple was placed in a small-sized amount of heat transfer paste as close as practical to the outlet of the MCF; in practice the distance between the thermocouple and the MCF exit was about 5 mm. A further *k*-type thermocouple was placed in the exit flow, such that the temperature of the emergent water could be measured. Water was supplied to the MCF at a flow-rate of 5 ml/min and the temperatures of the MCF surface and emergent water taken over a range of heater set-point temperatures.

A.2. Results and discussion

A plot of the volumetric average temperature of the water exiting the MCF as a function of the surface temperature of the MCF is shown in Fig. A2. Error bars in this plot have been set to ±1 °C to allow for thermocouple error.

This plot demonstrates that there is a linear relationship between the temperature of the fluid exiting the MCF and the MCF surface temperature, with extrapolation of the results revealing that the surface temperature and the fluid temperature were equal at 16 °C, the temperature of the laboratory during the experiment. Linear regression resulted in the correlation shown in the following equation:

$$T_{\text{fluid}} = 1.11T_{\text{surface}} - 1.7. \tag{A.1}$$

References

[1] D.B. Tuckerman, R.F.W. Pease, High performance heat sinking for VLSI, Electron Device Lett. 2 (5) (1981) 126–129.

[2] A. Weisberg, H.H. Bau, J.N. Zemel, Analysis of microchannels for integrated cooling, Int. J. Heat Mass Transfer 35 (10) (1992) 2465.

[3] B. Gromoll, Micro cooling systems for high density packaging, Rev. Gen. Therm. 37 (9) (1998) 781–787.

[4] C.H. Shen, C. Gau, Heat exchanger fabrication with arrays of sensors and heaters with its micro-scale impingement cooling process analysis and measurements, Sens. Actuators A 114 (2–3) (2004) 154–162.

[5] S. Belhardj, S. Mimouni, A. Saidane, M. Benzohra, Using microchannels to cool microprocessors: a transmission-line-matrix study, Microelectron. J. 34 (4) (2003) 247–253.

[6] H. Lee, Y. Jeong, J. Shin, J. Baek, M. Kang, K. Chun, Package embedded heat exchanger for stacked multi-chip module, Sens. Actuators A 114 (2–3) (2004) 204–211.

[7] C.R. Friedrich, S.D. Kang, Micro heat exchangers fabricated by diamond machining, Precision Eng. 16 (1) (1994) 56.

[8] P.X. Jiang, M.H. Fan, G.S. Si, Z.P. Ren, Thermal-hydraulic performance of small scale micro-channel and porous-media heat-exchangers, Int. J. Heat Mass Transfer 44 (5) (2001) 1039–1051.

[9] H.H. Bau, Optimization of conduits' shape in micro heat exchangers, Int. J. Heat Mass Transfer 41 (18) (1998) 2717–2724.

[10] Y.S. Muzychka, Constructal design of forced convection cooled microchannel heat sinks and heat exchangers, Int. J. Heat Mass Transfer 48 (15) (2005) 3119–3127.

[11] H. Hirshfeld, I. Silverman, A. Arenshtam, D. Kijel, A. Nagler, High heat flux cooling of accelerator targets with micro-channels, Nucl. Instrum. Methods Phys. Res., Sect. A 562 (2) (2006) 903–905.

[12] A. Jokar, M.H. Hosni, S.J. Eckels, Dimensional analysis on the evaporation and condensation of refrigerant R-134a in minichannel plate heat exchangers, Appl. Therm. Eng. 26 (17–18) (2006) 2287–2300.

[13] L. Jiang, M. Wong, Y. Zohar, Transient temperature performance of an integrated micro-thermal system, J. Micromech. Microeng. 10 (3) (2000) 466–476.

[14] R.H. Saiki, D.H. Gelfand, S. Stoffel, S.J. Scharf, R. Higuchi, G.T. Horn, K.B. Mullis, H.A. Erlich, Primer-directed enzymatic amplification of DNA with a thermostable DNA polymerase, Science 239 (4839) (1988) 487–491.

[15] S.H. DeWitt, Microreactors for chemical synthesis, Curr. Opin. Chem. Biol. 3 (3) (1999) 350–356.

[16] B. Hallmark, M.R. Mackley, F. Gadala-Maria, Hollow microcapillary arrays in thin plastic films, Adv. Eng. Mater. 7 (2005) 545–547.

[17] B. Hallmark, M.R. Mackley, F. Gadala-Maria, The melt processing of polymer microcapillary film (MCF), J. Non-Newtonian Fluid Mech. 128 (2–3) (2005) 83–98.

[18] C.H. Hornung, B. Hallmark, R.P. Hesketh, M.R. Mackley, The fluid flow and heat transfer performance of thermoplastic microcapillary films, J. Micromech. Microeng. 16 (2006) 434–447.

[19] OmegaEngineering, The Temperature Handbook, vol. 29, 1995.

[20] R.H. Perry, D.W. Green, J.O. Maloney, Perry's Chemical Engineers' Handbook, McGraw-Hill, New York/London, 1997.

[21] B. Hallmark, The experimental observation and numerical modeling of cast film deformation using novel capillary markers, Polym. Eng. Sci. 48 (1) (2008) 37–51.

[22] C.H. Hornung, I.R. Baxendale, S.V. Ley, M.R. Mackley, A novel microcapillary flow disc (MFD) reactor for organic synthesis, Org. Process Res. Dev. 11 (2007) 399–405.